JOURNAL OF GEOPHYSICAL RESEARCH, VOL. 96, NO. C11, PAGES 20,561–20,569, NOVEMBER 15, 1991

Breaking Waves Affecting Microwave Backscatter 2. Dependence on Wind and Wave Conditions

A. T. JESSUP[1] AND W. K. MELVILLE

R. M. Parsons Laboratory, Massachusetts Institute of Technology, Cambridge

W. C. KELLER

U.S. Naval Research Laboratory, Washington, D.C.

This paper is the second of a two-part series on using microwave techniques for detection and characterization of wave breaking. The statistics of sea spikes detected using the method described in Part 1 are investigated as functions of friction velocity u_* and of a Reynolds number Re_* based on u_* and the dominant surface wavelength. For vertical (VV) and horizontal (HH) polarization, the frequency of sea spikes and their contribution to the mean radar cross section show a roughly cubic dependence on u_*. The percentage of wave crests producing sea spikes, P_{ss}, is consistent with the Re_* exponent of 1.5 reported by other investigators. At high friction velocities (u_* between 40 and 50 cm s^{-1}), sea spikes contribute between 10% and 15% to the mean radar cross section for VV polarization and between 15% and 25% for HH polarization. The data suggest that the average radar cross section of an individual sea spike does not depend on u_*. Measurements of Doppler frequency and bandwidth are used to investigate the kinematics of the breaking process.

1. INTRODUCTION

In Part 1 [*Jessup et al.*, this issue] we showed that a detection scheme based on thresholds in radar cross section and Doppler bandwidth consistently identified individual breaking events. Here, in Part 2, statistics of the breaking events detected are compared with models and measurements of wave breaking by other investigators. Our analysis is based on measurements from the SAXON-CLT experiment (Synthetic Aperture Radar and X-Band Ocean Nonlinearities experiment at the Chesapeake Light Tower) which occurred in the fall of 1988. Most field measurements of wave breaking are based on the fraction of affected surface area, referred to as the whitecap coverage [*Monahan*, 1969, 1971; *Monahan and O'Muircheartaigh*, 1986; *Toba and Chaen*, 1973] (see also *Wu* [1988], *Monahan and Woolf* [1989], and *Wu* [1989]), which is expected to vary cubically with friction velocity [*Wu*, 1979]. An alternative measure for the degree of wave breaking is the percentage of breaking crests passing a fixed point. *Holthuijsen and Herbers* [1986] and *Toba et al.* [1971] used similar techniques to count the number of breaking crests identified visually by an observer. *Longuet-Higgins and Smith* [1983] and *Thorpe and Humphries* [1980] used wire wave gauges to detect abrupt changes in surface elevation attributed to breaking waves. *Weissman et al.* [1984] correlated increases in the energy of high-frequency waves with visual observations of breaking.

Toba and colleagues have proposed that the dependence of wave breaking on the combined effects of wind stress and wave conditions can be parameterized by a Reynolds number:

$$Re_* = \frac{u_* L}{\nu} \tag{1}$$

where u_* is the friction velocity, L is a length scale characteristic of the sea surface, and ν is the kinematic viscosity of air. The theoretical formulation [*Toba*, 1972] is supported by field measurements of whitecap coverage [*Toba and Chaen*, 1973] and wind tunnel measurements of the percentage of breaking crests [*Toba and Kunishi*, 1970]. For the field measurements, the whitecap coverage was proportional to $Re_*^{1.5}$, whereas we have estimated an Re_* exponent of 1.4 for their laboratory data.

A cubic dependence on u_* is equivalent to a $Re_*^{1.5}$ dependence if we assume the fetch-dependent scaling relation suggested by *Kitaigorodskii* [1970] and summarized by *Phillips* [1977]:

$$\frac{\omega_0 u_*}{g} \approx 2.2 \left[\frac{xg}{u_*^2}\right]^{-\frac{1}{4}} \tag{2}$$

where $\omega_0 u_*/g$ is the dimensionless frequency of the wave height spectral peak and xg/u_*^2 is the dimensionless fetch. The wavelength λ_0 corresponding to the peak frequency of the surface displacement spectrum is proportional to the friction velocity u_*:

$$\lambda_0 \approx \frac{5}{4}\left[\frac{x}{g}\right]^{\frac{1}{2}} u_* \tag{3}$$

when ω_0 in (2) is given by the deepwater dispersion relation. If λ_0 is used for the length scale L, then Re_* is proportional to u_*^2. Thus the Re_* exponent of 1.5 estimated by *Toba and Chaen* [1973] for the fraction of breaking crests is consistent with the cubic dependence on friction velocity found for other measures of wave breaking. Note that the Re_* based on λ_0 in (3) incorporates the friction velocity and fetch dependence into a single parameter. Thus a formulation in terms of Re_* effectively relaxes the constraint of a linear dependence of L on u_*.

In Part 1, we addressed the validity of using the frequency of sea spikes caused by individual breaking waves as a measure of the degree of wave breaking. *Phillips* [1988] predicted a cubic dependence on friction velocity for both the frequency of sea

[1] Presently at the Applied Physics Laboratory, University of Washington, Seattle, Washington.

Paper number 91JC01994.
0148-0227/91/91JC-01994$05.00

spikes and their contribution to the mean radar cross section. *Jessup et al.* [1990] presented the first quantitative analysis of sea spikes associated with breaking waves over a range of environmental conditions. Sea spikes likely to be associated with large-scale breaking events were identified by a cross section threshold based on Doppler frequency information and partially verified by video recordings. The dependence of the sea spike frequency on friction velocity and the contribution of sea spikes to the mean radar cross section were given for data collected in the North Sea. The results for that limited data set were consistent with *Phillips'* [1988] model.

Melville et al. [1988] and *Loewen and Melville* [1991] measured microwave scattering and sound generated by breaking waves controlled in a laboratory. The dissipation due to breaking correlated almost linearly with both the backscattered microwave power and the radiated acoustic power. These laboratory results and *Phillips'* [1988] analytical model suggest that information about the breaking process itself may be inferred from microwave measurements of breaking waves. If their results apply to field measurements, then microwave observations of breaking waves may yield important dynamic and acoustic information on the wave field and the upper ocean.

2. Results and Discussion

The results discussed in Part 1 showed that a microwave scatterometer cannot detect all waves that break near the illuminated area. However, the number of breaking waves detected using bandwidth information was approximately proportional to the total number of sea spikes caused by breaking waves (see Table 2, Part 1). Therefore if the number of sea spikes caused by breaking waves is a valid indicator of the degree of wave breaking, our method provides a relative measure of this phenomenon.

In Part 1 we tested four detection schemes based on radar cross section or bandwidth maxima (or both) corresponding to individual waves. The results in this paper are based on the scheme using both the radar cross section and bandwidth maxima, which detected the highest percentage of sea spikes caused by breaking waves. The edited data set consisted of thirty-eight 1-hour records covering various sea conditions (see section 2.3 and Table 1 in Part 1). The data were divided into seven subsets, called runs, made up of 1-hour records occurring close in time. We described the wave conditions for each run in terms of the number and location of major peaks in the wave height spectrum. Some of the spectra were unimodal and some bimodal. Unimodal spectra indicate seas dominated by either swell (runs 1 and 6) or wind waves (runs 11 and 12), whereas bimodal spectra indicate mixed seas (runs 4, 5, and 9). Bimodal spectra suggest the possibility of breaking due to the interaction of swell and wind waves.

To help identify variations that might be caused by the differing wave conditions, each of the seven runs is identified by a different symbol in the plots in this paper. Some of these results are presented on log-log plots fitted with a straight line illustrating a power law relation. These lines are the result of a least squares, orthogonal regression analysis, following the method described by *Casella and Berger* [1990]. Orthogonal regression is more appropriate than linear regression when both variables involved contain random errors. The analysis provides an exponent a which is a measure of the slope of the line, 95% confidence intervals on that slope, and a correlation coefficient ρ. The regression parameters for the detection scheme used are listed in Table 1. For comparison with *Phillips'* [1988] formulation, the power-law relations are expressed in terms of his dimensionless friction velocity $\tilde{u}_* = [u_*^2\kappa/g]^{1/4}$, where κ is the electromagnetic wave number and g is the acceleration of gravity. The plots of the computed quantities versus friction velocity have two x-axis scales: the top scale is the dimensional friction velocity u_* (cm s^{-1}), and the lower scale is the dimensionless friction velocity $\tilde{u}_*$.

TABLE 1. Least Squares, Orthogonal Regression Coefficients for Power Laws of Form $Y = C_i X^{a_i}$ Listed With 95% Confidence Limits and Correlation Coefficients ρ_i

Relation	Wave Conditions	a_i	$\log C_i$	ρ_i
N vs.u_*	unimodal	2.9±0.6	1.1	0.91
P_{ss} vs.Re_*	all	1.4±0.2	−7.0	0.94
	unimodal	1.2±0.3	−5.9	0.84
σ^0_{VV} vs.u_*	all	2.0±0.1	−2.1	0.98
σ^0_{HH} vs.u_*	all	1.9±0.1	−2.2	0.96
σ^0_{ss} (VV) vs.u_*	unimodal	3.2±0.7	−3.3	0.89
σ^0_{ss} (HH) vs.u_*	unimodal	3.2±0.8	−3.3	0.87

2.1. *Dependence on Wind and Wave Conditions*

The log-log plot in Figure 1*a* shows the dependence of the sea spike frequency N on friction velocity for the entire data set described in Part 1. Although N tends to increase with u_*, the amount of scatter suggests that a straight-line fit would be inappropriate. Note, however, that the scatter is characterized by clustering according to run number. The scatter is significantly reduced by excluding data with bimodal wave height spectra, as is shown in Figure 1*b*. In this case, a linear fit to the data seems reasonable; for the relation

$$N = C_1 \tilde{u}_*^{a_1} \tag{4}$$

the exponent a_1 (with 95% confidence limits) is 2.9±0.6, and the correlation coefficient ρ_1 is 0.91. Although these data cover a limited range of friction velocities and have relatively large confidence limits, they support *Phillips'* [1988] prediction of a cubic friction velocity dependence for the frequency of sea spikes. The results are comparable to our measurements from the North Sea [*Jessup et al.*, 1990], which had friction velocity exponents between 2.7 and 3.6 and correlation coefficients between 0.84 and 0.91. The decrease in scatter from Figure 1*a* to Figure 1*b* suggests that friction velocity alone does not adequately parameterize wave breaking.

The roughness Reynolds number Re_* incorporates both wind and wave conditions into a single parameter. The Re_* dependence of the percentage of wave crests producing sea spikes, P_{ss}, is shown for the entire data set in Figure 2*a* and for runs with unimodal spectra in Figure 2*b*. The characteristic wavelength L used in computing Re_* corresponded to the peak frequency of the surface displacement spectrum when computed using the dispersion relation. When the surface displacement spectrum was bimodal, the higher-frequency peak was used. In contrast to Figure 1, the scatter in Figure 2 is not significantly affected by excluding runs with bimodal spectra. The expression

$$P_{ss} = C_2 Re_*^{a_2} \tag{5}$$

yields an exponent a_2 of 1.4±0.2 (with 95% confidence limits)

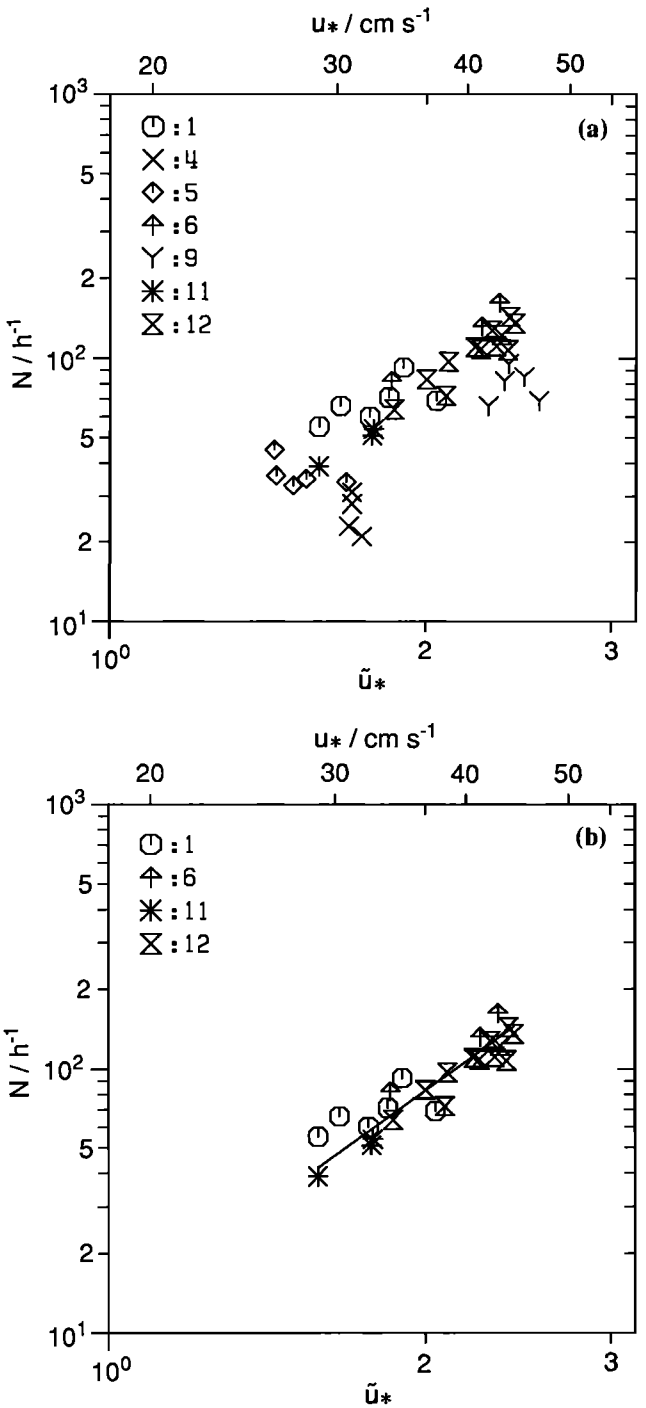

Fig. 1. Frequency of sea spikes, N (number per hour), versus friction velocity u_* for (*a*) all wave conditions and (*b*) unimodal wave conditions. The slope of the orthogonal regression line (with 95% confidence intervals) for Figure 1*b* is 2.9 ± 0.6 with a correlation coefficient of 0.91 (see equation 4 and Table 1). For this and similar plots, each symbol corresponds to 1 hour of data, with different symbols for each run (see Table 1, Part 1).

for the data in Figure 2*a* and 1.2 ± 0.3 for those in Figure 2*b*, with corresponding correlation coefficients ρ_2 of 0.94 and 0.84. These exponents compare reasonably well with the exponents of 1.4 and 1.5 found by *Toba and Kunishi* [1970] and *Toba and Chaen* [1973]. Note that although the Reynolds number includes dependence on wave conditions, it does not reflect the number of peaks in the wave height spectrum. Thus the reason for the better correlation for the entire data set is not obvious and simply may be a result of the larger range of Re_* in Figure 2*a*. Although the correlation coefficients for the regressions on u_* and Re_* are comparable, the greater dynamic range and improvement in confidence limits for Re_* suggest Re_* is better suited for parameterizing wave breaking than is u_*.

Previous authors have reported the wind dependence of P_{ss} in terms of U_{10}, the wind speed referenced to a height of 10 m. They based the total number of wave crests used in computing P_{ss} either on zero crossings in surface displacement measurements [*Holthuijsen and Herbers*, 1986] or on an average wave period [*Toba et al.*, 1971]. For our data, we define the total number of wave crests as the record length (in seconds) times f_{peak}, the frequency (in hertz) of the peak of the surface displacement spectrum. When the surface displacement spectrum was

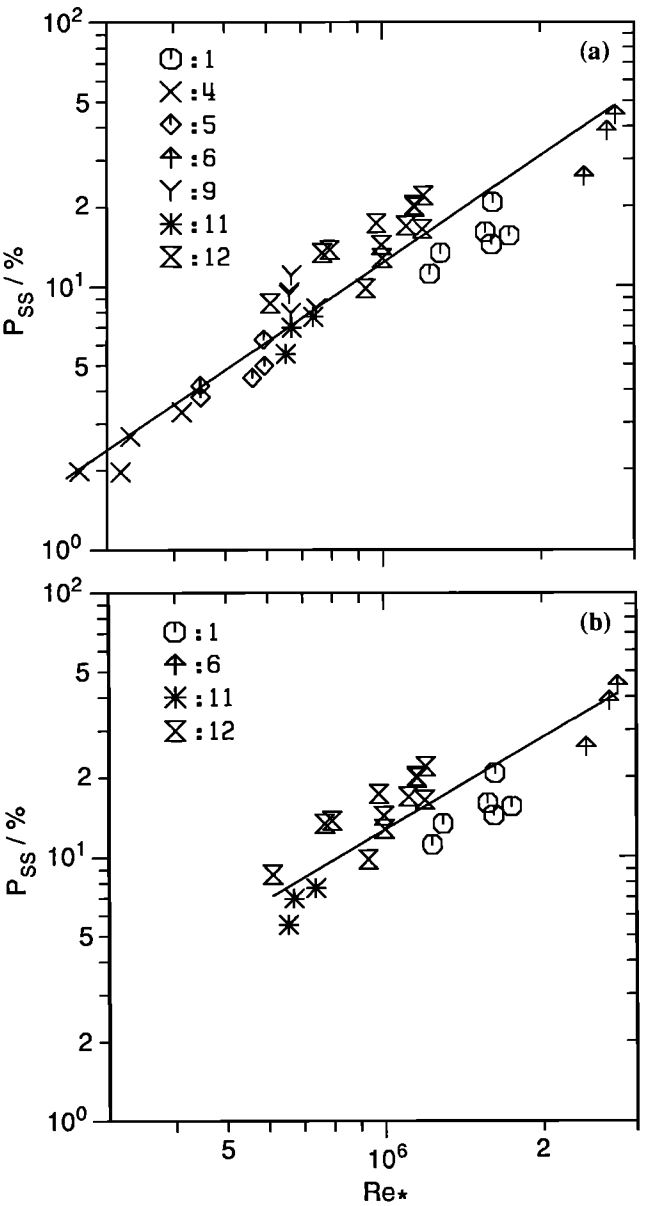

Fig. 2. Percentage of crests producing sea spikes, P_{ss}, versus the roughness Reynolds number Re_* for (*a*) all wave conditions and (*b*) unimodal wave conditions. The corresponding slopes of the orthogonal regression lines (with 95% confidence intervals) and correlation coefficients are 1.4 ± 0.2 and 0.94 in Figure 2*a* and 1.2 ± 0.3 and 0.84 in Figure 2*b* (see equation (5) and Table 1).

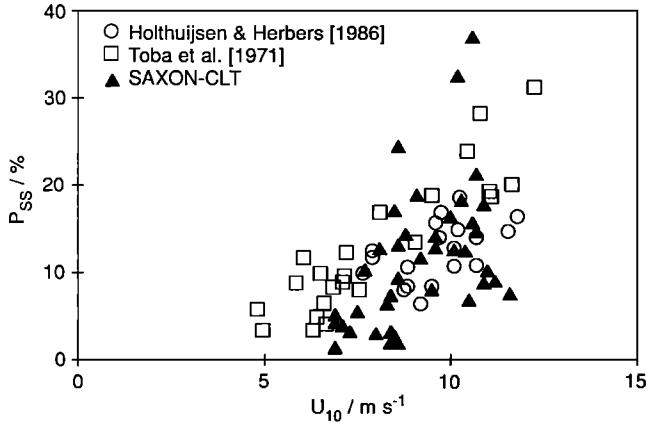

Fig. 3. Comparison of results for SAXON-CLT measurement (solid triangles) with those of *Holthuijsen and Herbers* [1986] (open circles) and *Toba et al.* [1971] (open squares) as a percentage of breaking crests versus U_{10}, the wind speed referenced to 10 m.

bimodal, the higher-frequency peak was used to determine f_{peak}. In Figure 3, we compare our measurements with the results reported by *Holthuijsen and Herbers* [1986] and *Toba et al.* [1971]. The previously published data (open symbols) and the SAXON-CLT data (solid triangles) are plotted on linear axes as the percentage of breaking crests P_{ss} versus U_{10}. Considering the inherent differences and uncertainties in the three measurements, we conclude that the agreement is reasonable.

2.2. *Mean and Sea Spike Radar Cross Sections*

The mean radar cross section σ^0 versus friction velocity is shown in Figure 4 for VV and HH polarization. The angle ϕ between the radar look direction and the wind direction ranged from 0° to 25° for the SAXON-CLT measurements. The expected variation of σ^0 with ϕ for ϕ in this range is less than 1 dB, according to the Seasat-A satellite scatterometer model SASS II [*Wentz et al.*, 1984]. The calibration accuracy of the scatterometer used in the SAXON-CLT experiment is estimated to be ±1 dB.

For

$$\sigma^0_{VV} = C_3 \tilde{u}_*^{a_3} \tag{6}$$

and

$$\sigma^0_{HH} = C_4 \tilde{u}_*^{a_4} \tag{7}$$

a_3 (with 95% confidence limits) and ρ_3 are 2.0±0.1 and 0.98, respectively, and a_4 and ρ_4 are 1.9±0.1 and 0.96.

We previously outlined two methods of computing the total sea spike contribution [*Jessup et al.*, 1990] which associated the individual sea spike contributions with the area under the spike above a specific value. For method 1, the lower bound was σ^0, the long-term mean radar cross section; for method 2 it was the smaller of the local minima on either side of the sea spike peak. In general, the contribution given by method 2 is slightly greater than that given by method 1. Because the friction velocity dependence is comparable using either method, only the results for method 2 are presented here.

Figure 5 shows the sea spike contribution σ^0_{ss} versus friction velocity for unimodal wave conditions. For VV polarization,

$$\sigma^0_{ss} = C_5 \tilde{u}_*^{a_5} \tag{8}$$

and for HH polarization,

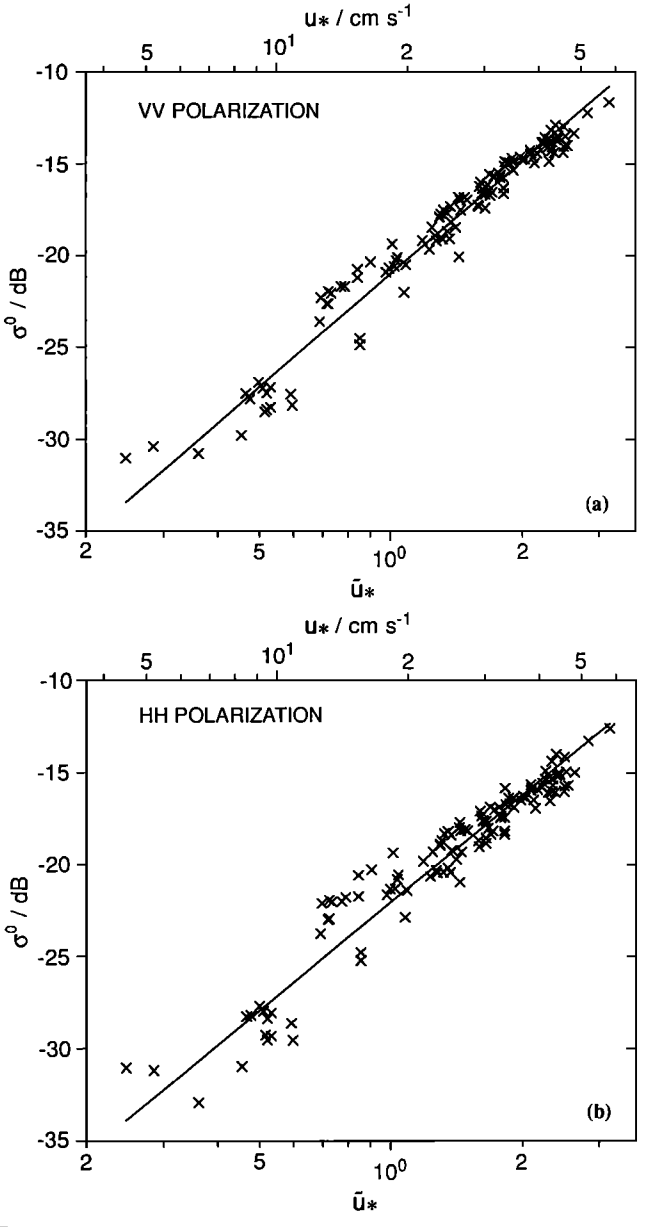

Fig. 4. Mean normalized radar cross section versus friction velocity for (*a*) VV and (*b*) HH polarization. Each symbol represents a 1-hour average. For VV polarization the slope of the orthogonal regression line (with 95% confidence intervals) is 2.0±0.1 and correlation coefficient ρ = 0.98; for HH polarization the slope is 1.9±0.1 and ρ = 0.96 (see equations (6) and (7)).

$$\sigma^0_{ss} = C_6 \tilde{u}_*^{a_6} \tag{9}$$

the exponents (with 95% confidence limits) are a_5 = 3.2±0.7 and a_6 = 3.2±0.8; the correlation coefficients are ρ_5 = 0.89 and ρ_6 = 0.87. These results support *Phillips'* [1988] prediction and are comparable to results reported by *Jessup et al.* [1990] of exponents between 3.3 and 3.8 and correlation coefficients between 0.88 and 0.93. Note that the values for σ^0_{ss} are roughly equal for VV and HH polarization, which is consistent with a sea spike polarization ratio of unity.

The roughly cubic dependence on friction velocity of both σ^0_{ss}, the sea spike contribution to the mean radar cross section, and N, the sea spike frequency, implies that these two quantities may be linearly related. Such a linear relationship suggests that the average radar cross section of an individual sea spike, σ^0_{ss}/N, might be

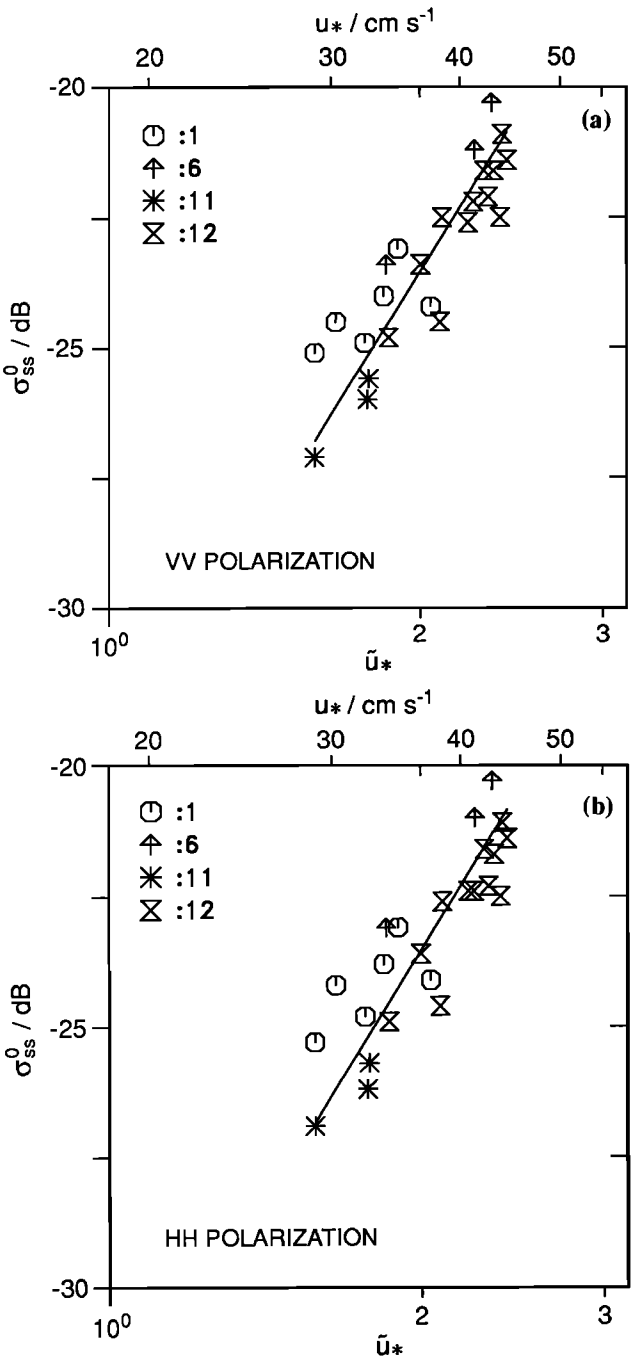

Fig. 5. Sea-spike contribution σ^0_{ss} versus friction velocity for unimodal wave data for (*a*) VV and (*b*) HH polarization. The slopes of the orthogonal regression lines (with 95% confidence intervals) and the correlation coefficients are 3.2 ± 0.7 and 0.89 and 3.2 ± 0.8 and 0.87 for VV and HH polarization, respectively (see equations (8) and (9) and Table 1).

independent of friction velocity [*Jessup et al.*, 1990]. The quantity σ^0_{ss}/N for the SAXON-CLT measurements is plotted as a function of friction velocity in Figure 6 for VV and HH polarizations. The scatter of approximately ±1 dB indicates that the average contribution of an individual sea spike is independent of u_*.

This suggests that the probability density function $p(\sigma^0_{ss})$ may also be independent of u_*. Figure 7 shows linear plots of $p(\sigma^0_{ss})$ for VV and HH polarization. The distributions include all runs and cover friction velocities of 25 to 45 cm s^{-1} in 5 cm s^{-1} intervals. The changes in the distributions are relatively small, and the centroids of the distributions, corresponding to the average individual cross sections, do not vary significantly with friction velocity.

The relative importance of σ^0_{ss} is of interest because current models of microwave backscatter from the ocean surface generally do not include returns from breaking events [*Donelan and Pierson*, 1987]. Figure 8 shows the dependence of the fractional sea spike radar cross section σ^0_{ss}/σ^0 on friction velocity for VV and HH polarization for all wave conditions. For HH polarization the detected sea spikes contribute almost 25% of the received power, whereas for VV polarization they contribute only about 15%. (The maximum contributions calculated using method 1 are approximately 5% less than these calculated using method 2.) A greater fractional sea spike contribution for HH

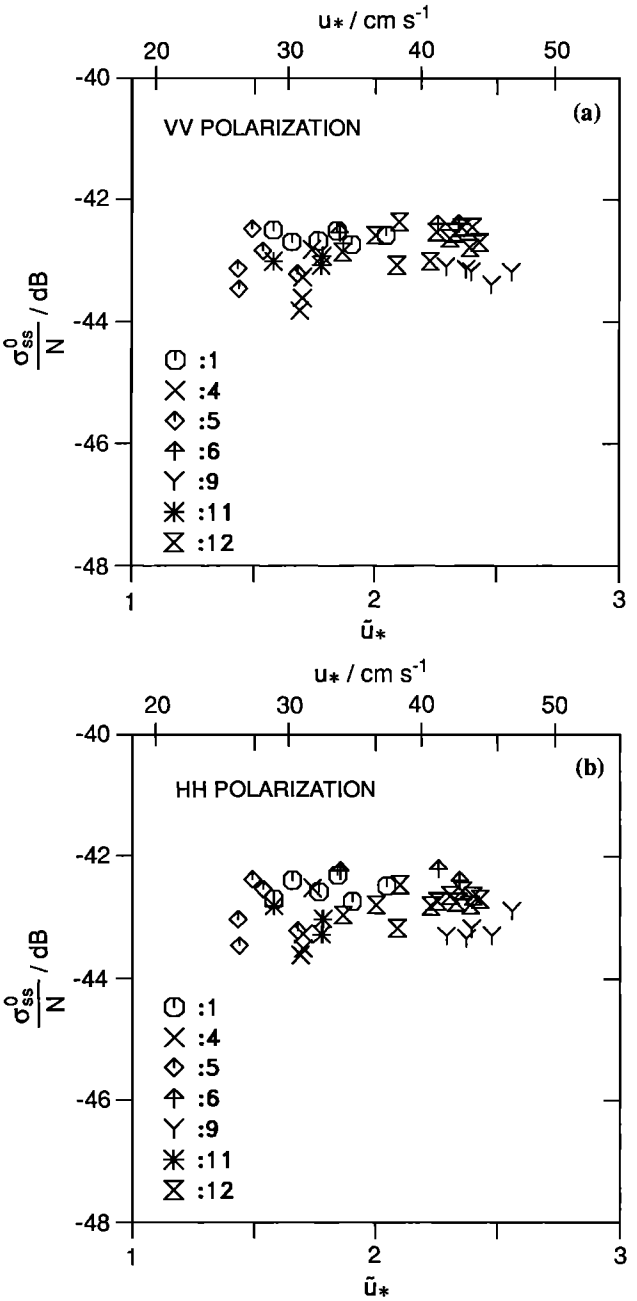

Fig. 6. Average sea spike contribution σ^0_{ss}/N versus friction velocity for (*a*) VV and (*b*) HH polarization for all data from Part 1. The scatter of approximately ±1 dB indicates that the average contribution of an individual sea spike is independent of friction velocity.

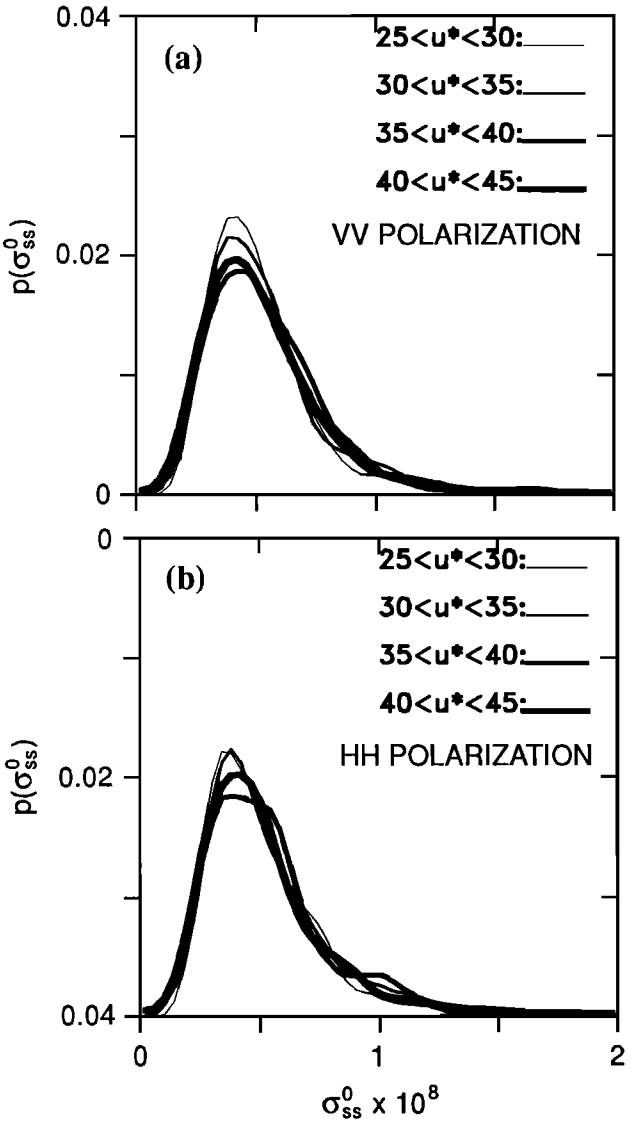

Fig. 7. Probability density functions for σ^0_{ss} for (*a*) VV and (*b*) HH polarization covering the friction velocity range 25–45 cm s^{-1} in 5 cm s^{-1} intervals for the data used in Figure 6. The invariance of the distributions is consistent with Figure 6.

polarization than for VV polarization is consistent with a polarization ratio that is greater than unity in the mean but near unity for individual sea spikes associated with breaking. These results agree with previous maximum contributions of 10% and 20% calculated using method 1 for VV and HH polarization, respectively [*Jessup et al.*, 1990].

2.3. *Kinematics of the Breaking Process*

When the illuminated area is small compared with the wavelength of the dominant surface wave, the Doppler frequency provides a measure of the sea surface velocity. For nonbreaking waves, the measured velocity is dominated by the line-of-sight orbital velocity of the long surface waves. For breaking waves we expect that the fluid-particle velocity at the crest is comparable to the phase speed [*Loewen and Melville*, 1991]. This suggests that the phase speed of the dominant surface wave may be an appropriate parameter for scaling Doppler velocity measurements of breaking waves.

As is shown in Part 1, maxima in the mean Doppler frequency tend to be correlated with large spikes in the radar cross section attributed to breaking waves. The average of the maximum mean Doppler velocity (i.e., the maximum first moment of the Doppler spectrum) corresponding to detected sea spikes $\bar{U}_{max}$ is given by

$$\bar{U}_{max} = \frac{1}{N}\sum_{i=1}^{N} U_{max} \tag{10}$$

where U_{max} is the line-of-sight velocity corresponding to the maximum mean Doppler frequency associated with a sea spike. The scaling of this average velocity associated with the detected breaking events may be relevant to the kinematics of the break-

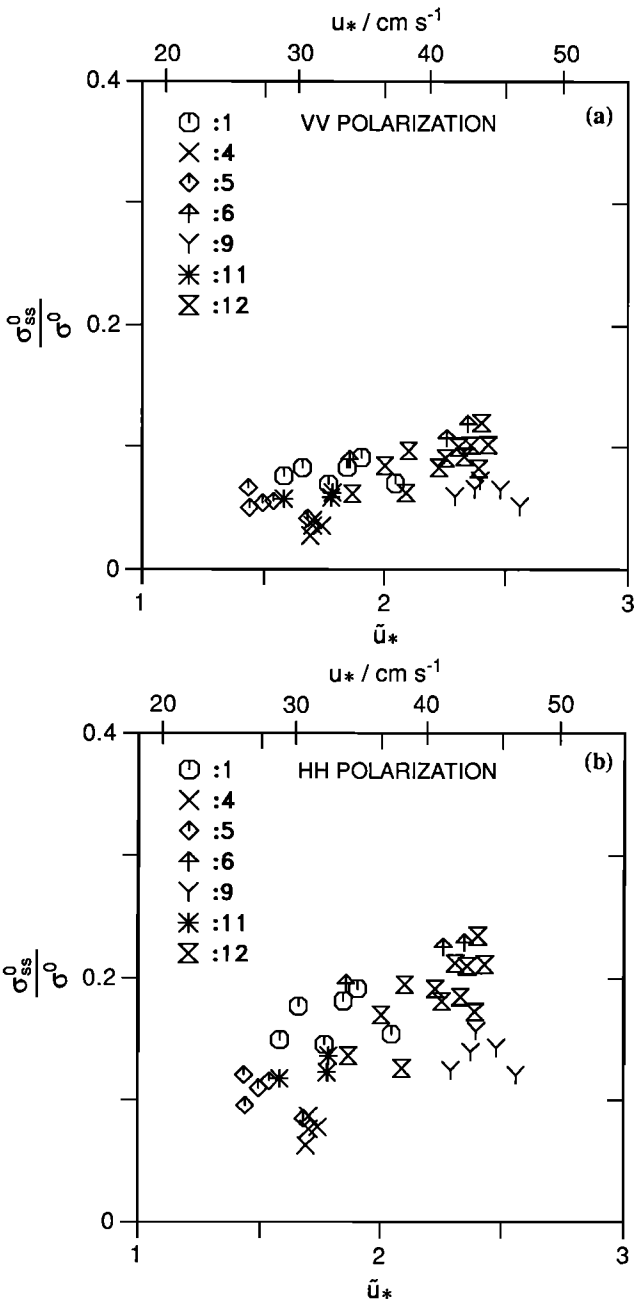

Fig. 8. Fractional radar cross section σ^0_{ss}/σ^0 versus friction velocity for (*a*) VV and (*b*) HH polarization. The detected sea spikes contribute nearly 15% and 25% of the cross section for VV and HH polarization, respectively.

ing process. If the average velocity is dominated by the large velocities within the whitecap region, it may indicate the scale of the breaking. Since we expect that the velocity near the crest of a breaking wave is nearly horizontal, we have assumed that $\bar{U}_{max}$ is due to a completely horizontal velocity. Furthermore, since the crest velocity of a breaking wave is expected to be comparable to its phase speed, we normalized $\bar{U}_{max}$ by C_{peak}, the phase speed corresponding to the peak of the surface displacement spectrum. When the surface displacement spectrum was bimodal, the higher-frequency peak was used to determine C_{peak}.

The dependence of $\bar{U}_{max}/C_{peak}$ on friction velocity is shown in Figure 9 for all wave conditions. The data show a moderate amount of scatter, with the values generally clustered near $\bar{U}_{max}/C_{peak} = 0.25$. Considering that the crest velocity of a breaking wave should be roughly equal to its phase speed, we might expect a value of $\bar{U}_{max}/C_{peak}$ closer to unity. However, $\bar{U}_{max}$ cannot be interpreted as the average velocity of the breaking crests. Because the Doppler spectrum reflects the power-weighted distribution of scatterer velocities within the illuminated area, the influence of the whitecap velocity on the mean frequency, or first moment, depends on the location of the breaking crest with respect to the illuminated area. Other factors affecting the relationship between the first moment and the whitecap velocity include the crest's orientation and the target strength of the breaking region relative to that of other sources of scattering. Thus $\bar{U}_{max}$ does not necessarily reflect the whitecap velocity.

Examples of Doppler spectra for times of maximum bandwidth (Figures 9 and 10 in Part 1) showed large velocities associated with the crest region of breaking waves. Because of the spectra's large bandwidth, however, the mean Doppler frequency was significantly less than the maximum Doppler frequency. The Doppler spectrum in Figure 10 of this paper dramatically illustrates that the whitecap velocity, although measured by the scatterometer, may not be reflected in the mean Doppler frequency.

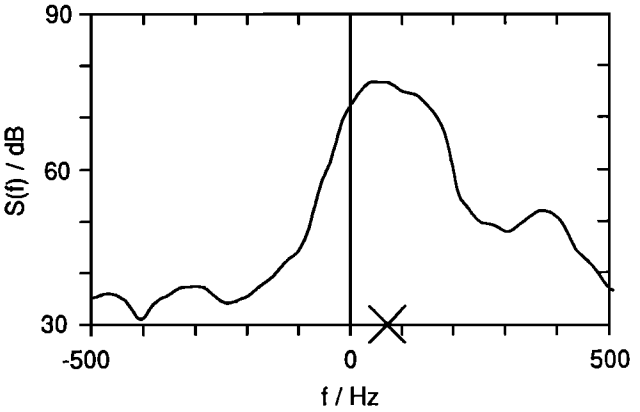

Fig. 10. Doppler spectrum $S(f)$ showing the signature of a fast-moving splash caused by a breaking wave. The frequency of the rightmost peak near 400 Hz corresponds to a line-of-sight velocity of roughly 4 m s^{-1}. The splash has a negligible effect on the mean Doppler frequency, which is less than 100 Hz and is indicated by an X on the abscissa.

This spectrum includes the Doppler signature of a fast-moving splash that occurred when the crest of a breaking wave was thrown forward and down into its forward face. The line-of-sight velocity corresponding to the frequency of the small peak on the right is roughly 4 m s^{-1}. This translates into a horizontal velocity of 5.7 m s^{-1}, which is near the phase speed of roughly 8 m s^{-1} based on the peak frequency of the wave height spectrum. Because the relative target strength of the splash is so low, it has a negligible effect on the mean Doppler velocity, which is approximately 0.7 m s^{-1}.

The bandwidth of the Doppler spectrum indicates the range of scatterer velocities within the illuminated area. In Part 1, large jumps in the bandwidth were found to be associated with the

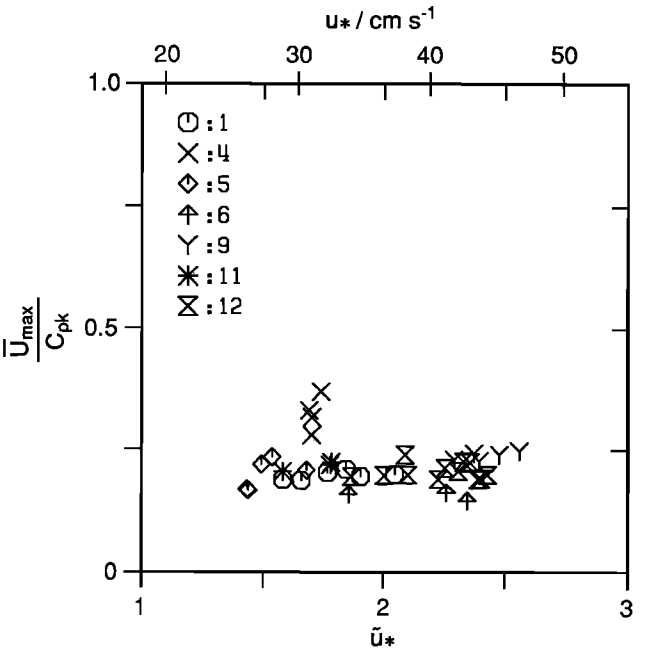

Fig. 9. Average maximum mean Doppler velocity $\bar{U}_{max}$ (see equation (10)) associated with detected sea spikes normalized by C_{peak}, the phase speed corresponding to the peak of the surface displacement spectrum. That $\bar{U}_{max}$ is about 25% of C_{peak} indicates that the mean Doppler frequency of detected breaking events is not dominated by the large velocities associated with whitecaps.

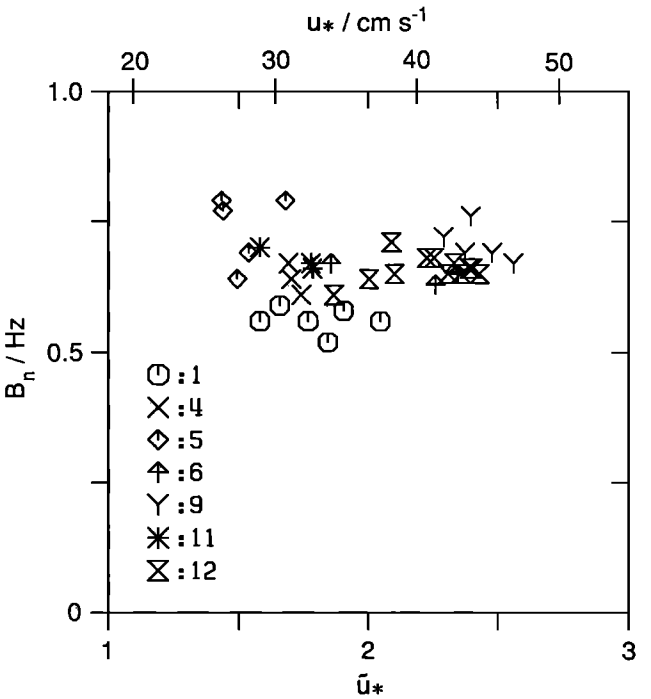

Fig. 11. Average normalized bandwidth (see equations (11) and (12)) associated with detected sea spikes. The values indicate that, on average, the maximum bandwidth associated with the detected events is roughly 50%–75% of the maximum mean Doppler frequency.

crest of breaking waves. We computed a normalized bandwidth B_n to investigate the scaling of the bandwidth maxima associated with breaking waves. For each event detected, we normalized the bandwidth maximum by the corresponding maximum mean Doppler frequency F_{max} associated with the event:

$$B_n = \frac{B_{max}}{F_{max}} \tag{11}$$

For each 1-hour record, the average normalized bandwidth $\bar{B}_n$ of the detected events is then

$$\bar{B}_n = \frac{1}{N} \sum_{i=1}^{N} \left[\frac{B_{max}}{F_{max}} \right]_i \tag{12}$$

where N is the total number of events detected. Figure 11 shows the variation of $\bar{B}_n$ with friction velocity u_* for all wave conditions. On average, the maximum bandwidth associated with the detected events is roughly 50–75% of the maximum mean Doppler frequency. The average (dimensional) bandwidths corresponding to the sea-spike maxima were 60–70 Hz. Degraded azimuthal resolution in synthetic aperture radar images has been associated with localized scatterer coherence times of the order of 10^{-2} s [*Lyzenga and Shuchman*, 1983]. The reciprocal of the average bandwidth associated with the detected sea spikes is of this same order.

3. Summary and Conclusion

Thirty-eight hours of data from the SAXON-CLT experiment were analyzed using the microwave technique outlined in Part 1 for detecting breaking events. The dependence of the detected events on wind and wave conditions was compared with the dependence calculated for other measurements of wave breaking and with analytical models. The contribution of sea spikes to the mean radar cross section was computed. Finally, measurements of the Doppler frequency and bandwidth were used to investigate the kinematics of the breaking process.

The frequency of sea spikes, N, was computed as the number of events in a 1-hour record. The roughly cubic dependence of N on friction velocity for unimodal wave conditions supports *Phillips*' [1988] model and is consistent with theoretical modeling and field measurements of whitecap coverage. The dependence of the percentage of breaking crests producing sea spikes, P_{ss}, on a roughness Reynolds number Re_* was relatively insensitive to the shape of the wave height spectrum and was consistent with laboratory and field measurements. An Re_* exponent of 1.5 was shown to be equivalent to a cubic friction velocity dependence using a fetch-dependent scaling law.

The dependence on friction velocity of the sea-spike contribution σ^0_{ss} to the mean radar cross section also supports *Phillips*' [1988] model. The fractional power for high friction velocities (40–50 cm s^{-1}) was between 10% and 15% for VV polarization and between 20% and 25% for HH polarization. These findings support the inclusion of wave breaking in scattering models, especially for HH polarization and high friction velocities. The data also suggest that the average radar cross section of an individual sea spike does not depend on u_*.

The average of the maximum mean Doppler velocities associated with the detected sea spikes was roughly 25% of the phase speed corresponding to the peak of the surface displacement spectrum. This indicates that the mean Doppler frequency of detected breaking events is not dominated by the large velocities associated with whitecaps. A normalized bandwidth associated with the detected events ranged between 0.50 and 0.75 and showed no functional dependence on friction velocity.

In conclusion, our investigation shows that the microwave detection of individual wave breaking events can be used as a meaningful measure of the degree of wave breaking.

Acknowledgments. In addition to the help acknowledged in Part 1, we thank the anonymous reviewer who pointed out the appropriateness of orthogonal regression over linear regression.

References

Casella, G., and R.L. Berger, *Statistical Inference*, p. 584, Wadsworth and Brooks/Cole Advanced Books and Software, Pacific Grove, Calif., 1990.

Donelan, M., and W.J. Pierson, Jr., Radar scattering and equilibrium ranges in wind-generated waves with application to scatterometry, *J. Geophys. Res.*, *92*(C5), 4971–5092, 1987.

Holthuijsen, L.H., and T.H.C. Herbers, Statistics of breaking waves observed as whitecaps in the open sea, *J. Phys. Oceanogr.*, *16*, 290–297, 1986.

Jessup, A.T., W.C. Keller, and W.K. Melville, Measurements of sea spikes in microwave backscatter at moderate incidence, *J. Geophys Res.*, *95*(C6), 9679–9688, 1990.

Jessup, A.T., W.K. Melville, and W.C. Keller, Breaking waves affecting microwave backscatter, 1, Detection and verification, *J Geophys. Res.*, this issue.

Kitaigorodskii, S.A., *Fizika Vzaimodestviya Atmosferi I Okeana (Physics of Air-Sea Interaction)*, Gidrometeorologicheskoe Izdatel'stvo, Leningrad, 1970. (English translation, Israel Program for Scientific Translation, Jerusalem, 1973.)

Loewen, M.R., and W.K. Melville, Microwave backscatter and acoustic radiation from breaking waves, *J Fluid Mech.*, *224*, 601–623, 1991.

Longuet-Higgins, M.S., and N.D. Smith, Measurement of breaking waves by a surface jump meter, *J. Geophys. Res.*, *88*, 9823–9831, 1983.

Lyzenga, D.R., and R.A. Shuchman, Analysis of scatter motion effects in Marsen X band SAR imagery, *J. Geophys. Res.*, *88*, 9769–9775, 1983.

Melville, W.K., M.R. Loewen, F.C. Felizardo, A.T. Jessup, and M.J. Buckingham, Acoustic and microwave signature of breaking waves, *Nature*, *336*, 54–59, 1988.

Monahan, E.C., Laboratory comparison of freshwater and saltwater whitecaps, *J. Geophys. Res.*, *74*, 6961–6966, 1969.

Monahan, E.C., Oceanic whitecaps, *J. Phys. Oceanogr.*, *1*, 139–144, 1971.

Monahan, E.C., and I.G. O'Muircheartaigh, Whitecaps and the passive remote sensing of the ocean surface, *Int. J. Remote Sens.*, *7*, 627–642, 1986.

Monahan, E.C., and D.K. Woolf, Comment on "Variations of whitecap coverage with wind stress and water temperature," *J. Phys. Oceanogr.*, *19*, 706–709, 1989.

Phillips, O.M., *The Dynamics of the Upper Ocean*, p. 161, Cambridge University Press, New York, 1977.

Phillips, O.M., Radar returns from the sea surface—Bragg scattering and breaking waves, *J. Phys. Oceanogr.*, *18*, 1065–1074, 1988.

Thorpe, S.A., and P.N. Humphries, Bubbles and breaking waves, *Nature*, *283*, 463–465, 1980.

Toba, Y., Local balance in the air-sea boundary processes, 1, On the growth process of wind waves, *J. Oceanogr Soc. Jpn*, *28*, 109–121, 1972.

Toba, Y., and M. Chaen, Quantitative expression of the breaking of wind waves on the sea surface, *Rec. Oceanogr. Works Jpn.*, *12*, 2–11, 1973.

Toba, Y., and H. Kunishi, Breaking of wind waves and the sea surface wind stress, *J. Oceanogr. Soc. Jpn.*, *26*, 71–80, 1970.

Toba, Y., H. Kunishi, K. Nishi, S. Kawai, Y. Shimada, and N. Shibata, Study on air-sea boundary processes at the Shirahama Oceanographic Tower Station, Disaster Institute, (in Japanese with English abstract) *Kyoto Univ Ann.*, *148*, 519–531, 1971.

Weissman, M.A., S.S. Atakturk, and K.B. Katsaros, Detection of breaking events in a wind-generated wave field, *J. Phys. Oceanogr.*, *14*, 1608–1619, 1984.

Wentz, F.J., S. Peteherych, and L.A. Thomas, A model function for ocean radar cross sections at 14.6 GHz, *J. Geophys. Res.*, *89*(C3), 3689–3704, 1984.

Wu, J., Oceanic whitecaps and sea state, *J. Phys. Oceanogr.*, *9*, 1064–1068, 1979.
Wu, J., Variations of whitecap coverage with wind stress and water temperature, *J. Phys. Oceanogr.*, *18*, 1448–1453, 1988.
Wu, J., Reply, *J. Phys. Oceanogr.*, *19*, 710–711, 1989.

A. T. Jessup, Applied Physics Laboratory, College of Ocean and Fishery Sciences, University of Washington, 1013 NE 40th Street, Seattle, WA 98105.
W. C. Keller, U.S. Naval Research Laboratory, Washington, DC 20375.
W. K. Melville, R. M. Parsons Laboratory, Massachusetts Institute of Technology, Cambridge, MA 02139.

(Received January 3, 1991;
revised July 29, 1991;
accepted July 29, 1991.)